How PtOx/CeO2 Nanostructures Catalyze CO Oxidation at Very Low Temperatures

ACS Catalysis

pubs.acs.org/acscatalysis

Research Article

How PtO_x/CeO_2 Nanostructures Catalyze CO Oxidation at Very Low Temperatures

Pablo Castro-Latorre, Albert Bruix,* Henrik Grönbeck, and Konstantin M. Neyman*

Cite This: *ACS Catal.* 2026, 16, 12009−12020

Read Online

ACCESS | Metrics & More | Article Recommendations | Supporting Information

ABSTRACT: Nanomaterials based on Pt and ceria (CeO_2) that are subjected to oxidative pretreatments can catalyze the CO oxidation reaction at temperatures below 0 °C, which is relevant for the conversion of low-temperature combustion emissions. However, the mechanisms by which such systems catalyze the low-temperature CO oxidation reaction remain unclear; the apparent activation energies measured experimentally for Pt/CeO_2 catalysts active below 0 °C are low and inconsistent with the activation barriers calculated using density-functional theory (DFT) on various oxidized or reduced ceria-supported Pt models. This study demonstrates, by means of DFT modeling and kinetic Monte Carlo simulations, CO oxidation pathways on stable ceria-supported PtO_x clusters involving activation energies, turnover frequencies, and reaction temperature onsets consistent with low-temperature experimental catalytic data. These reaction pathways involve the oxidation of CO with O atoms of the supported PtO_x clusters instead of those from the CeO_2 support often suggested for Mars van Krevelen mechanisms on ceria-supported metal catalysts. In contrast to the often-assumed higher reactivity of interface sites, the low-temperature CO oxidation mechanism via top-layer O atoms of the Pt_6O_9 cluster distant from the support exhibits higher turnover frequencies than the mechanism involving interface O atoms of the cluster. These mechanistic insights pave the way for designing very low-temperature oxidation catalysts based on stable supported metal-oxide clusters.

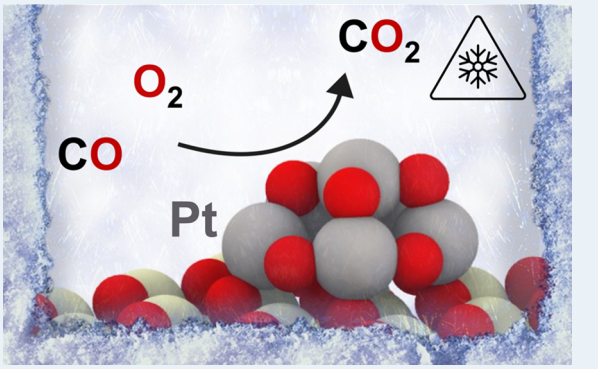

KEYWORDS: *Pt/CeO_2 catalysts, low-temperature CO oxidation, PtO_x clusters, DFT calculations, kinetic monte carlo*

1. INTRODUCTION

Oxidation reactions are important for the conversion of toxic exhaust gases.[1,2] CO oxidation is also an important probe reaction for obtaining fundamental insights into heterogeneous catalysis.[3,4] Significant efforts have been devoted to developing efficient CO oxidation catalysts with materials ranging from noble metals[5,6] to oxide-based formulations.[7,8] Among the latter, cerium dioxide (CeO_2, ceria)[9] has been widely used as a supporting material for more active metal components due to its capacity to store oxygen and enable prominent metal-support interactions that affect the chemical properties of supported metal particles and clusters.[10−15]

An important challenge is to lower the temperature required for CO oxidation light-off down to very low-temperature regimes.[16] Pt is a common active component of efficient low-temperature oxidation catalysts, which, when supported on CeO_2, can form such diverse structures as single atoms,[17−21] small clusters,[22−25] and nanoparticles.[26,27] This structural diversity contributes to the multiple factors controlling the catalytic activity of Pt, including the oxidation states of Pt atoms,[28−31] the geometry of CeO_2 surface facets,[32] the modification of the CeO_2 support by dopants,[33,34] or the mixing with other oxides.[35,36] Pt deposited on ceria can also easily form oxidized PtO_x species,[37−44] whose presence was related to CO oxidation catalytic activity at temperatures as low as −40 °C and measured apparent activation energies of ∼0.1 to 0.4 eV.[38,43,45]

Langmuir-Hinshelwood (LH)[46,47] mechanisms involving adsorbed oxygen or Mars van Krevelen (MvK)[48−50] mechanisms involving instead oxygen in the catalyst structure are commonly invoked to explain how the CO oxidation activity depends on numerous electronic and structural features of Pt/CeO_2 catalysts under varying reaction conditions.[26,51,52] However, as was demonstrated in the exhaustive Density Functional Theory (DFT) study from Koleva et al.,[22] either LH or MvK mechanisms proposed in the literature for both reduced[46−48,50] and oxidized[40,53] Pt particles and atoms involve rate limiting elementary steps with higher activation barriers than those consistent with CO oxidation activity below 0 °C.

Received: February 5, 2026
Revised: May 13, 2026
Accepted: May 14, 2026
Published: June 11, 2026

https://doi.org/10.1021/acscatal.6c01003
ACS Catal. 2026, 16, 12009−12020

For example, an activation energy of ∼0.9 eV such as that reported by Koleva et al.,[22] Bosio et al.,[52] and others,[46,48,53] for the MvK mechanism on ceria-supported reduced Pt particles results in noticeable catalytic activity only well above room temperature in kinetic Monte Carlo (kMC) simulations.[52] Somewhat lower barriers for the CO oxidation step ranging from ∼0.4 to 0.7 eV were reported on models with high CO coverage on ceria-supported Pt particles[27,48,50,54] and for atomically dispersed Pt cations[27,45,48,53,55−58] on ceria surfaces and nanoparticles. In fact, the barrier for the CO oxidation step in such systems depends strongly on the nature of the oxidant, with the Ce^{4+} oxidants within ceria resulting in higher barriers than $Pt^{\delta+}$ cations or $[Pt_n]^{\delta+}$ clusters.[22] This observation is consistent with the low-temperature oxidation occurring over oxidized PtO_x clusters on ceria and, indeed, mechanisms calculated by means of DFT by Wang et al.[38] for such systems involve low barriers of ∼0.3 eV for the elementary step where CO is oxidized with an O atom of the PtO_x cluster. However, Wang et al. calculated that O_2 activation on PtO_x and O mobility within the cluster become rate determining steps with barriers >0.9 eV. Steps related to the activation and dissociation of O_2 also become rate-determining on the atomically dispersed Pt cations and Pt particles under high CO coverages, except for cases in which the CeO_2 support is already reduced and exhibits (endothermically formed) O vacancies that can activate O_2.[22] Given the discrepancy between these quite large barriers and the experimentally measured activity at temperatures below 0 °C of oxidized ceria-supported PtO_xnew mechanistic insights on ceria-supported PtO_x catalysts are required for an atomic-level understanding of such remarkable low-temperature activity.

In this work, DFT calculations and kMC simulations are performed to evaluate the activity of ceria-supported PtO_x clusters towards CO oxidation. Different reaction mechanisms on a $CeO_2(111)$-supported Pt_6O_9/CeO_2 structural model are proposed to rationalize activity of this catalyst at very low temperature. Several explored catalytic paths show that the reaction proceeds by CO oxidation steps, where O is provided by the ceria-supported Pt_6O_9 cluster or adsorbed and activated O_2 molecules. The resulting activation barriers are notably lower than those requiring direct involvement of O atoms from the CeO_2 support. Activity data from the kMC simulations provide turnover frequencies consistent with the experimentally observed CO oxidation activity at temperatures lower than 0 °C attributed to ceria-supported PtO_x particles.

2. COMPUTATIONAL DETAILS

2.1. Computational Methods

Spin-polarized DFT calculations were performed with the Vienna Ab-initio Simulation Package (VASP).[59−61] The valence electrons-2*s* and 2*p* of C and O atoms, 5*d* and 6*s* of Pt atoms and 5*s*, 5*p*, 6*s*, 5*d* and 4*f* of Ce atoms-were described explicitly by a plane wave basis set with a cutoff energy of 415 eV. Interactions between valence and core electrons were accounted for using the projector augmented wave (PAW) method.[62] The PW91[63] generalized gradient approximation exchange-correlation functional was used corrected with a Hubbard *U*-term[64] for Ce*4f* electrons, with $U = 4.0$ eV.[65] The Brillouin zone was sampled using only the Γ point.

Electronic structure convergence criterion was 5.0×10^{-6} eV and geometry optimizations were considered converged, when forces acting on each relaxed atom became smaller than 0.05 eV/Å. Transition state structures were calculated using the climbing image nudge elastic band method.[66] Vibrational frequencies were calculated to confirm that the identified minima and saddle points were stationary points of the potential energy surface and to calculate zero-point energy corrections and Gibbs energies.

2.2. Structural Model of Ceria-Supported PtO_x

We use a Pt_6O_9 cluster supported on the $CeO_2(111)$ surface (Figure 1) as the structural model for ceria-supported PtO_x. In previous work,[37] this supported cluster model was identified as the most stable state of cluster structures comprising 6 Pt atoms under a wide range of conditions (including very slightly oxidizing conditions and temperatures up to 500 K) by means of an exhaustive global optimization and ab initio thermodynamics. This cluster is characterized by a network of $[PtO_4]$ structural motifs, where each Pt atom exhibits a square-planar coordination environment. We note that for the Pt atoms in interface positions, the $[PtO_4]$ motif is completed with O atoms of the ceria lattice. The $CeO_2(111)$ support was represented by a periodic slab with 2 O–Ce–O tri-layers and a 4×4 surface supercell with 12 Å of vacuum between neighboring slabs. In all DFT calculations, atoms of the O–Ce–O tri-layer in contact with the Pt_6O_9 cluster were allowed to relax while keeping the bottom tri-layer atoms fixed in their bulk positions corresponding to the experimental lattice parameter of 5.40 Å. Using a thicker $CeO_2(111)$ slab with structural relaxation of more O–Ce–O tri-layers in contact with Pt_6O_9 may slightly affect the energy of the cluster-support interaction, but no significant changes of the individual Pt–O bonds are expected from such model extension.

2.3. Kinetic Simulations

Kinetic Monte Carlo (kMC) simulations were performed using the first reaction method (FRM)[67] as implemented in the MonteCoffee package.[68] Within the FRM, the time at which an event connects two states α and β of a given system is:

$$t_{\alpha\beta} = t - \frac{1}{W_{\beta\alpha}} \ln(r) \tag{1}$$

where t is the simulation time, $W_{\beta\alpha}$ is the rate constant of a specific event and r is a uniform random number on the unit interval. Events are stored in an event list and when the first event of the list is executed, the state of the system is updated along with the simulation time. Following the execution of an event, some events in the event list are disabled, while other new events are enabled.

For adsorption events, the rate constant W^{ads} is calculated using collision theory:

$$W^{ads} = \frac{PA}{\sqrt{2\pi m k_B T}} \tag{2}$$

Here, P is the partial pressure of the adsorbate, A is the area of the adsorption site, m is the mass of the adsorbate,

https://doi.org/10.1021/acscatal.6c01003
ACS Catal. 2026, 16, 12009−12020

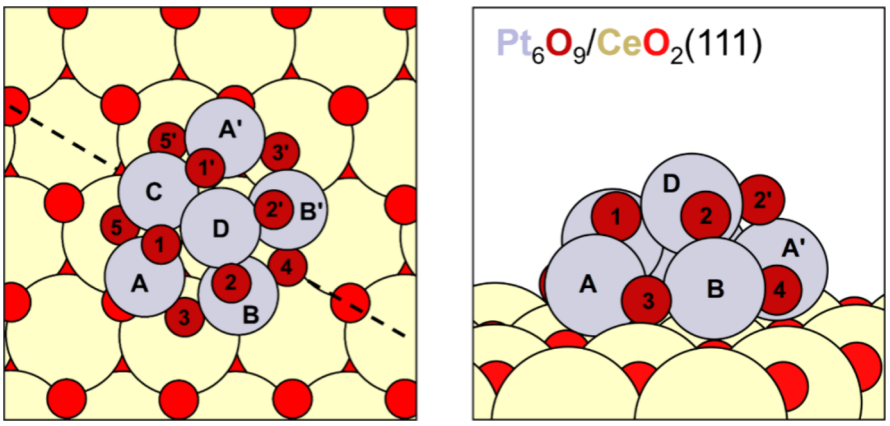

Figure 1. Globally optimized structure of Pt_6O_9 cluster supported on $CeO_2(111)$ surface: top view − left panel, side view − right panel. Color coding of atoms: Pt-grey, O of Pt_6O_9 − dark red, O of CeO_2 − light red, Ce − beige. In the Pt_6O_9 cluster Pt atoms are labeled with capital letters and O atoms with digits. The dashed line displays a symmetry plane of the cluster, which makes the corresponding atoms with primed and not primed labels equivalent.

k_B is Boltzmann constant and T is the temperature. For activated reactive events such as formation of intermediates or activated desorptions (e.g. some CO_2 desorption steps as shown below), the expression used is the following:

$$W_j = \frac{k_B T}{h} e^{\frac{-E_j}{k_B T}} \quad (3)$$

where h is Planck constant and E_j is the activation energy of the process j. If j corresponds to a non-activated desorption event, E_j is the adsorption energy.

kMC simulations allow us to account for the spatial distribution and connectivity of different sites. While the active sites of Pt on the Pt_6O_9 cluster are considered to be independent from each other (i.e. diffusion of adsorbates between active sites is neglected) in our simulations, we define a list of neighbors for every Pt atom from surrounding O atoms and the possible reactive or diffusive events involving these Pt and O sites for every given state. The simulations were carried out for a total simulation time of 0.1 s, which is long enough to ensure convergence of the turnover frequency (TOF) in the range of −100 to 100 °C. Given the stochastic nature of the kMC approach, 10 simulations were run for each temperature with different random initialization seeds to ensure statistical accuracy and significance.

3. RESULTS AND DISCUSSION

3.1. CO Adsorption

The reactivity of the Pt_6O_9 cluster on $CeO_2(111)$ has been probed through the adsorption of a CO molecule on various sites of the cluster calculated from different initial positions of CO. These local-minimum adsorption structures correspond to CO bound to the cluster via Pt atoms. Some geometry relaxations of CO on O sites of the PtO_x cluster converged directly to the CO_2-like structures described below. However, the formation of such complexes involves the breaking of a Pt–O bond and is therefore activated process (as shown by the corresponding calculated barriers reported below). The resulting adsorption energies $E_{ads}(CO)$ (see Table 1) were calculated as.

$$E_{ads}(CO) = E(CO_{top} - Pt_6O_9/CeO_2) - E(Pt_6O_9/CeO_2) - E(CO)$$

where $E(CO_{top}–Pt_6O_9/CeO_2)$ and $E(Pt_6O_9/CeO_2)$ are the total energies of the CeO_2-supported Pt_6O_9 with and without CO adsorbed in on-top positions of Pt atoms, respectively. $E(CO)$ is the total energy of the gas-phase CO molecule. Negative values therefore correspond to thermodynamically favorable adsorption. The results in Table 1 show that adsorption is stronger on atoms C and D, i.e. those which form square planar $[PtO_4]$ motifs with O atoms only of the PtO_x cluster. Adsorption on Pt atoms that use one O atom of the ceria lattice to form such motifs is less favorable.

3.2. O Vacancy Formation

After the adsorption of a CO molecule on a Pt site, oxidation could occur through a MvK mechanism by consuming an oxygen atom provided by the reducible CeO_2 support[22,52] or the oxygen-rich Pt_6O_9 cluster. To evaluate reactivity of the O atoms of the supported PtO_x cluster, the O vacancy formation energy $E(O^v)$ for O atoms of the Pt_6O_9 cluster on $CeO_2(111)$ was calculated (see Table 2).

As shown in Figure 1, the O^1 and O^2 atoms have no direct bonds to the CeO_2 support and are therefore hitherto referred to as top-layer O atoms, while O^3, O^4 and O^5 atoms, which form bonds with the support, are referred to as bottom-layer or interface O atoms. The top-layer O atoms are thermodynamically easier to remove than the bottom-layer ones (i.e., they have lower $E(O^v)$, see Table 2), indicating that it is more favorable to distort/reduce the $[PtO_4]$ motifs that do not include any O from the ceria support. Importantly, $E(O^v)$ in the Pt_6O_9 cluster is lower than in the $CeO_2(111)$ support near or distant from Pt_6O_9, as calculated in previous work for $CeO_2(111)$-supported Pt clusters,[69] which indicates that O atoms from the PtO_x cluster are more reactive than those of the $CeO_2(111)$ surface. Notably, the deposited Pt_6O_9 cluster does not decrease the calculated O vacancy formation energy of the support compared

https://doi.org/10.1021/acscatal.6c01003
ACS Catal. 2026, 16, 12009−12020

Table 1. Adsorption Energy $E_{ads}(CO)$ of One CO Molecule in On-Top Sites of Different Pt Atoms of the Pt_6O_9 Cluster on the $CeO_2(111)$ Surface (See Figure 1 for Labels of the Pt Atoms)[a]

Pt atom	$E_{ads}(CO)$, eV
C	−0.86
D	−0.83
A (A')	−0.69
B (B')	−0.19

[a]Given the symmetry of the cluster, $E_{ads}(CO)$ for each pair of the primed and non-primed Pt atoms are equal. The resulting optimized structures for each site are shown in Figure S5.

Table 2. O Vacancy Formation Energy $E(O^v)$ for the Pt_6O_9 Cluster on the $CeO_2(111)$ Surface (see Figure 1 for Labels of the O Atoms)[a]

O atom	$E(O^v)$, eV
2 (2')	1.71
1 (1')	1.76
5 (5')	1.92
4	2.17
3 (3')	2.23

[a]These $E(O^v)$ are notably lower than 3.02 eV calculated using our model for removal of a surface O atom of $CeO_2(111)$ closest to the Pt^A atom, which is representative of $E(O^v)$ values for the interface O atoms of $CeO_2(111)$. The optimized structures for each vacancy site are shown in Figure S5.

to that of the bare $CeO_2(111)$ surface.[69] Furthermore, creating an O vacancy in the $PtO_x/CeO_2(111)$ system does not lead to the formation of Ce^{3+} centers, neither by removing an O atom from the ceria surface nor from the PtO_x. The two electrons left behind by the removed O atom are therefore shared by various Pt atoms of the cluster, as evidenced by the extra electron charge of ca. 0.8 |e| (in terms of the Bader charges, Figure S4) being distributed over Pt atoms near the created O vacancy in the PtO_x cluster. Interestingly, the −0.8 |e| Bader charge of O atoms of the PtO_x cluster is less negative than that of O atoms in the CeO_2 surface, indicating a less pronounced ionicity of Pt–O bonds compared to Ce–O bonds. This less ionic character of O in PtO_x cluster is directly related to the higher reducibility of the PtO_x cluster with respect to the CeO_2 surface.

3.3. 1st O–CO Complex Formation and CO_2 Desorption

We therefore explore reaction paths for oxidation of the adsorbed CO molecule by the O atoms of the Pt_6O_9 cluster, leading to the activated O–CO complexes as illustrated in Figure 2, which exhibit a bent structure typical of carbonite-like structures.

The reaction energies from adsorbed CO to bent O–CO are calculated as.

$$\Delta E_r(O-CO) = E(O-CO-Pt_6O_8/CeO_2) - E(CO_{top}-Pt_6O_9/CeO_2)$$

where $E(O–CO–Pt_6O_8/CeO_2)$ is the total energy of the O–CO complex on Pt_6O_8/CeO_2 and $E(CO_{top}–Pt_6O_9/CeO_2)$ is the total energy of CO adsorbed on top of a Pt atom in Pt_6O_9/CeO_2. The $CO_{top}–Pt_6O_9/CeO_2$ and $O–CO–Pt_6O_8/CeO_2$ states are separated by an energy barrier $E^{\neq}$, which has been characterized with transition state search calculations for different combinations of Pt and O atoms. The energy of the subsequent CO_2 desorption is calculated as.

$$\Delta E_{des}(CO_2) = E(Pt_6O_8(v\#)/CeO_2) + E(CO_2) - E(O-CO-Pt_6O_8/CeO_2)$$

where $E(Pt_6O_8(v\#)/CeO_2)$ is the total energy of a Pt_6O_8/CeO_2 complex with # specifying the O atom removed from the cluster when desorbing CO_2. $E(CO_2)$ is the total energy of a gas-phase CO_2 molecule. The calculated energies related to several O–CO and CO_2-desorbed states along with the associated reaction and transition state energies separating CO and O–CO structures ($\Delta E_r(O–CO)$, $E^{\neq}(CO\rightarrow O–CO)$) and O–CO and CO_2 desorbed structures ($\Delta E_{des}(CO_2)$, $E^{\neq}(CO_2\ _{des})$) are collected in Table 3.

The formation of the O–CO complexes from adsorbed CO on Pt is an energetically favorable process stabilizing the system by 1.0–1.8 eV. Activation barriers for this process are from 0.1 to 0.5 eV. Notably, using Pt_6O_9 as the source of oxygen atoms for CO oxidation results in much lower activation energies compared to the 0.9−1.0 eV activation energies calculated for ceria-supported Pt particles[22,52] and PtO_x clusters[38] in previous studies. The present CO_2 desorption energies $\Delta E_{des}(CO_2)$, −0.38 to 0.24 eV, show that CO_2 desorption from this activated state O–CO is energetically feasible, but may involve an energy barrier. We have therefore calculated the transition state for CO_2 desorption from the 1D O–CO complex structure (the state following the lowest-barrier O–CO formation) and obtained an energy barrier of 0.36 eV.

Our calculations also reveal that the adsorption of CO can lead to carbonate-like CO_3 species involving two O atoms (2 and 2') of the Pt_6O_9 cluster, and which are by 0.16 eV more stable than the O–CO complex on the 2D site (see Table 3). However, the calculated reaction barriers (see Figure S1) from CO on site D to O–CO on site 2D (0.52 eV) and subsequently to the CO_3 complex (0.77 eV) are significantly higher than those starting from the same CO on site D to form O–CO on site 1D (0.30 eV) and subsequently to desorb into gas-phase CO_2 (0.36 eV). The desorption energy of CO_2 from the CO_3-like complex is low (0.42 eV), indicating that temperatures able to overcome the 0.77 eV barrier to form the CO_3 species will also be able to eliminate them by desorbing gas-phase CO_2.

3.4. 2nd O–CO Complex Formation and CO_2 Desorption

The oxidation of the first CO molecule and desorption of CO_2 result in the formation of a partially reduced Pt_6O_8/CeO_2 with a vacancy in the top-layer O^1 or the bottom-layer O^3 atom sites, given the low activation barriers for CO_2 release from these sites.

Two main reaction paths are conceivable starting from these Pt_6O_8/CeO_2 structures given that the reoxidation or further reduction processes of the Pt_6O_8 cluster are competitive events. The first path (Path #1) involves first the reoxidation of the cluster by an O_2 molecule adsorbed at the vacancy site, which results in a Pt_6O_{10} cluster with an "extra" O atom available for oxidation of the next adsorbed CO molecule. The sequence in which reactants adsorb for this path is

https://doi.org/10.1021/acscatal.6c01003
ACS Catal. 2026, 16, 12009−12020

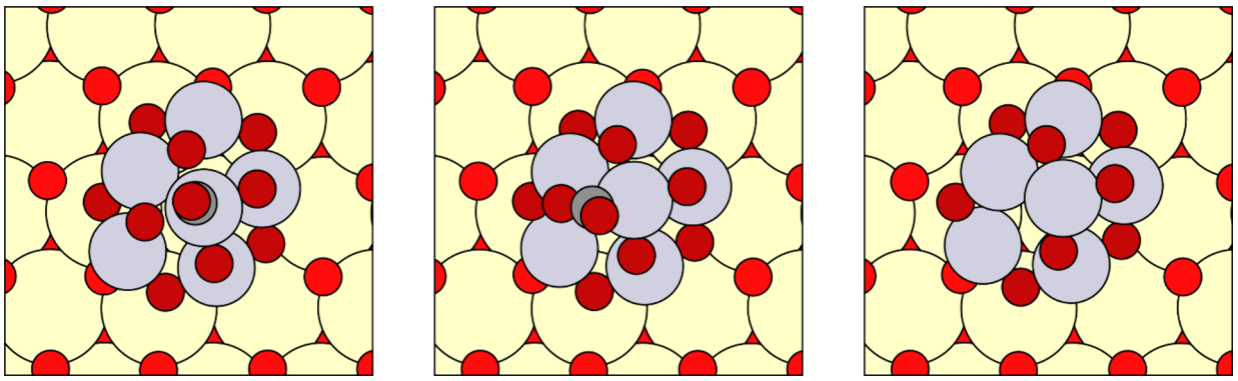

Figure 2. Schematic representation of CO oxidation via the formation of an O–CO complex. The left-hand side panel show s CO adsorbed on- top of a Pt atom, in the central panel the O–CO complex has been formed, while in the right-hand panel CO_2 has desorbed creating a vacancy in the Pt_6O_9 cluster. Color coding of atoms: Pt-grey, O of Pt_6O_9 and CO − dark red, O of CeO_2 − light red, Ce − beige.

Table 3. Energies (in eV) Characterizing Activated O–CO Complexes on Pt_6O_9/CeO_2[a]

O–CO/Pt	ΔE_f(O–CO)	$E^{\neq}$(CO→O–CO)	ΔE_r(O–CO)	$E^{\neq}(CO_{2\ des})$	$\Delta E_{des}(CO_2)$
1A	−1.23	0.32	−0.54		−0.30
1C	−1.15	0.45	−0.29		−0.38
1D	−1.38	0.30	−0.55	0.36	−0.14
2D	−1.82	0.52	−0.99		0.24
3A	−1.24	0.10	−0.55		0.19
5A	−1.03	0.43	−0.34		−0.33
5C	−1.49	0.39	−0.63		0.13
CO_3	−1.99		−1.16		0.41

[a]The O–CO/Pt sites are coded by the labels of the O atom reacting with CO and of the Pt atom on which CO is adsorbed (see Figure 1). E.g., the notation 1A means that the O^1 and Pt^A atoms form the O–CO complex. ΔE_f(O–CO) is the formation energy of O–CO/Pt from gas-phase CO and clean Pt_6O_9. ΔE_r(O–CO) is the formation energy of O–CO/Pt from the on-top adsorbed CO and O atom of Pt_6O_9, $E^{\neq}$(CO→O–CO) is the activation energy for this reaction, and $\Delta E_{des}(CO_2)$ is the desorption energy of CO_2 with respect to O–CO/Pt with the corresponding activation barrier $E^{\neq}(CO_{2\ des})$. All adsorption structures are shown in Figure S5. See more calculated activation barriers in Table S3.

therefore CO→O_2→CO. The second path, termed CO→CO→O_2 or Path #2 (Figure S2), involves adsorption of a second CO molecule on the Pt_6O_8 cluster after the desorption of the first formed CO_2, the further reduction of Pt_6O_8 to Pt_6O_7 after desorbing a second CO_2 molecule, and the final re-oxidation of the remaining Pt_6O_7 to Pt_6O_9 by adsorption and dissociation of an O_2 molecule, completing the catalytic cycle.

In both reaction paths #1 and #2, the adsorptions of CO and O_2 at/near the created v1 and v3 vacancy sites of the Pt_6O_8 cluster are competitive events. Adsorption energies for CO on these sites are shown in Table 4 (see the structures in Figure S5). Adsorption on such vacancy sites can lead to adsorption complexes where the CO molecules are located on-top of a Pt atom (Pt^Av1, Pt^Cv1, and Pt^Av3), forming a O–CO type complex ($Pt^{2D}v1$), or on bridging positions between two Pt atoms (Pt^C–Pt^Dv1). Here, v1 and v3 indicate the location of the I vacancy. Adsorption energies of an O_2 molecule on the v1 and v3 vacancies of the Pt_6O_8 cluster are −1.67 eV and −1.84 eV, respectively. Adsorption of O_2 is therefore stronger than CO adsorption on all sites except Pt^Av3, which exhibits a strong interaction with CO and could therefore become poisoned. The adsorbed O_2 molecule acquires −0.84 |e| (according to Bader charges), becoming activated and with an elongated O–O bond of length 1.44 Å, close to that of the O–O bond in an H_2O_2 molecule (1.45 Å).

Table 4. Adsorption Energy E_{ads}(CO) of a Second CO Molecule on Pt Atoms near O Vacancies V1 And V3 of the Pt_6O_8 Cluster Formed after Oxidation of a First CO Molecule[a]

site	E_{ads}(CO), eV
Pt^Av1	−1.26
Pt^Cv1	−0.64
$Pt^{2D}v1$	−1.50
Pt^C–Pt^Dv1	−1.50
Pt^Av3	−2.39

[a]The resulting optimized structures for each site are shown in Figure S5.

3.5. Path #1

For path #1 (CO→O_2→CO), we evaluate the adsorption of CO on different sites of the Pt_6O_8 cluster with an already adsorbed O_2 molecule (i.e. on O_2–Pt_6O_8 or Pt_6O_{10}). Calculated adsorption energies on Pt sites adjacent to the adsorbed O_2 of the O_2–Pt_6O_8(v1) and O_2–Pt_6O_8(v3) structures (where v1 and v3 indicate the location of the O vacancy that the O_2 molecule is adsorbed on) are given in Table 5, together with reaction energies to form the activated O–CO complexes, CO_2 desorption energies, and the corresponding energy barriers. On the Pt^Av3 site, the adsorption energy of

https://doi.org/10.1021/acscatal.6c01003
ACS Catal. 2026, 16, 12009−12020

Table 5. Adsorption Energies and Activation Barriers (in eV) Characterizing the Formation of Activated O–CO Complexes on Pt_6O_8/CeO_2 (i.e., Exhibiting an O Vacancy) with an Adsorbed O_2 Molecule[a]

site	E_{ads}(CO)	$E^{\neq}$(CO→O–CO)	ΔE_r(O–CO)	$E^{\neq}$(CO_2 des)	ΔE_{des}(CO_2)
Pt^Av1	−0.49			0.76[b]	−2.88
Pt^Cv1	−0.43	0.99	−0.88		2.06
Pt^Dv1	−0.51	0.17	−1.10	0.33	−1.76
Pt^Av3	−0.52			0.56	−3.16

[a]Adsorption energies E_{ads}(CO) of CO on Pt sites of Pt_6O_{10} (i.e. O_2–Pt_6O_8) near an O_2 molecule adsorbed on v1 or v3 vacancy sites. $E^{\neq}$ is the activation energy for the O–CO formation, $\Delta E_{des}(CO_2)$ is the energy of CO_2 desorption with respect to O–CO/Pt_6O_9. The resulting optimized structures for each site are shown in Figure S5. [b]The transition state structures corresponding to these relatively high activation barriers were optimized with a lower accuracy.

CO is slightly smaller in magnitude than the activation energy for O–CO formation on the same site, implying that CO desorption and O–CO complex formation are competitive. For Pt^Av1 and Pt^Cv1 sites, desorption of CO would be kinetically favored with respect to O–CO formation. At variance, on the Pt^Dv1 site the activation barrier for O–CO formation is noticeably smaller (of just 0.17 eV) than the energy for CO desorption from this site (0.51 eV), indicating that this site is involved in the low-temperature oxidation of CO. Furthermore, the transition state for CO_2 desorption from the Pt^Dv1 O–CO complex (0.36 eV) is also lower than the desorption energy of CO.

We note that CO adsorption is generally weaker in the presence of the adsorbed O_2 (i.e., on Pt sites of the O_2–Pt_6O_8 cluster) than on the original Pt_6O_9 cluster (see Table 1). This is probably due to the strong interaction of the O_2 molecule with the vacancy site (which involves such Pt atoms) and other coordination and steric effects that weaken coadsorption of CO and O_2.

3.6. Path #2

As mentioned above, path #2 (Figure S2) involves adsorption of a second CO molecule on the Pt_6O_8 cluster after the desorption of the first formed CO_2, the further reduction of Pt_6O_8 to Pt_6O_7 after desorbing a second CO_2 molecule, and the final re-oxidation of the remaining Pt_6O_7 to Pt_6O_9 by adsorption and dissociation of an O_2 molecule, completing the catalytic cycle. The second CO oxidation proceeds by the adsorption of the second CO molecule on the Pt^{2D}v1 (see Table 4). The adsorbed CO molecules can then react with an O atom in position 2 with a barrier of 0.63 eV, which directly produces the desorbed CO_2 molecule instead of the activated O–CO complex. An O_2 molecule can then very favorably adsorb on the vacancy sites, $E_{ads} = -1.94$ eV, spontaneously leading to the dissociation of O_2 and healing of both O vacancies. The highest barrier 0.63 eV for this path (oxidation of the second CO molecule) seems inconsistent with the very low-temperature catalytic activity. The fact that this path #2, which reduces Pt_6O_9 to Pt_6O_7 before reoxidation, involves significantly larger barriers than path #1, which reduces Pt_6O_9 only to Pt_6O_8 before reoxidation, indicates the kinetic stability of the Pt_6O_9 cluster to reduction beyond Pt_6O_8. Furthermore, O_2 binds very strongly (with E_{ads} ranging from −1.6 to −3.6 eV) to single or double O vacancies formed on the Pt_6O_9 cluster, which disfavors the weaker adsorption of CO on these sites required for further cluster reduction. Thus, more significant reduction of the PtO_x cluster is less kinetically favored than the moderate O removal along the reaction path.

3.7. Path #3

Finally, one can define a third path #3 analogous to path #1, with a CO→O_2→CO reactant sequence, but where the first adsorbed CO is oxidized instead of an O atom from the top layer of Pt_6O_9 by an O atom from the bottom layer of Pt_6O_9 (i.e., by an interface O atom). The catalytic cycles involving O atoms from the top or bottom O-layers of the Pt_6O_9 cluster are also referred to as top-layer (see Figure 3) and bottom-layer (see Figure 4) cycles, respectively. The elementary step with the highest barrier for the top-layer cycle is the desorption of the first CO_2 from the formed O–CO complex, with an energy barrier of 0.36 eV, while the second O–CO complex formation and CO_2 desorption have lower barriers of 0.17 and 0.33 eV, respectively. For the bottom-layer cycle, oxidation of the first CO molecule to form the O–CO complex has a barrier of 0.10 eV, followed by a 0.19 eV CO_2 desorption energy in a barrierless process. In turn, the highest barrier for the oxidation of the second CO molecule, which directly results in desorbed CO_2 instead of activated O–CO, is 0.56 eV. Thus, reactions at the interface are less kinetically favored than those at layers of the PtO_x particle not in direct contact with the ceria surface. This indicates that MvK mechanisms at the PtO_x/ceria interface are less kinetically favored, not only due to the high activation barriers reported for the MvK mechanism on metallic Pt particles supported on CeO_2 using O atoms of the ceria lattice but also for MvK mechanisms involving O atoms in the oxidized Pt cluster.[22,52]

For an overview, all elementary reaction steps studied in the present work for paths #1, #2 and #3, along with the corresponding structures and reaction energies are summarized as a reaction network in Figure 5.

3.8. KMC Simulations

In order to connect the calculated kinetic parameters with quantitative turnover frequencies, we use the calculated data as input for kinetic Monte Carlo (kMC) simulations as outlined in Section 2.3. Two additional system-specific approximations are assumed in the present kMC simulations: (i) interactions between adsorbates not explicitly considered in the DFT calculations are ignored and (ii) only low CO coverages (one CO molecule per ceria-supported Pt_6O_9 cluster) are considered independently of the CO pressure. The average adsorption energy of a single CO molecule adsorbed on either the A, A', C and D sites of the Pt_6O_9 cluster is −0.77 eV (Table 1). When these four sites are simultaneously occupied by four adsorbed CO molecules (high-coverage CO adsorption), the average adsorption energy per CO molecule strongly decreases

https://doi.org/10.1021/acscatal.6c01003
ACS Catal. 2026, 16, 12009−12020

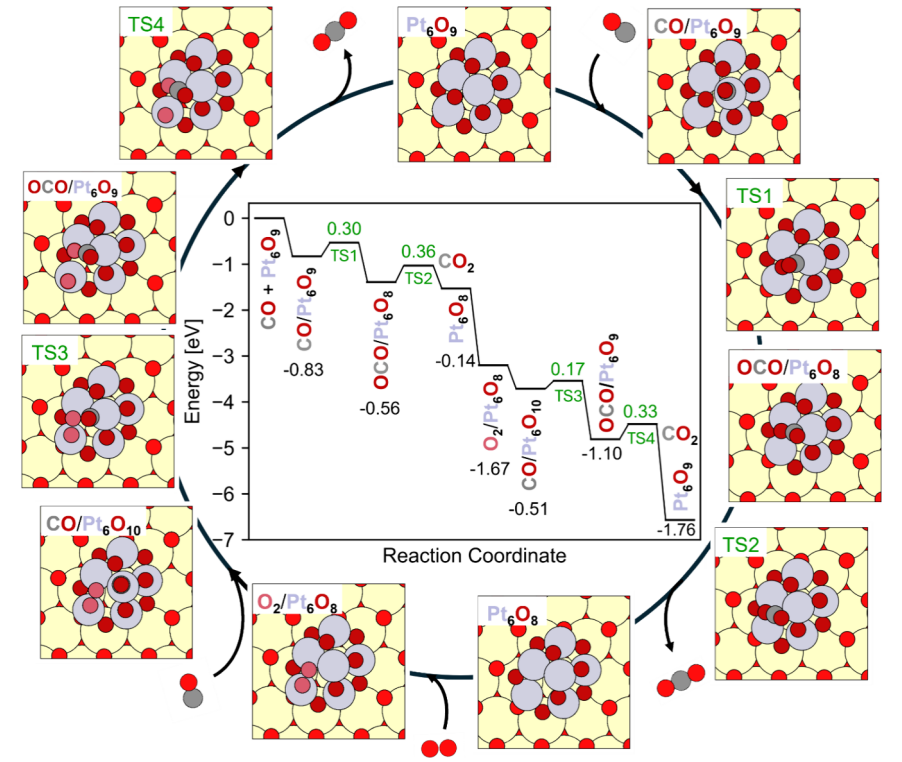

Figure 3. Calculated energies and structures of path #1 for CO oxidation on the $Pt_6O_9/CeO_2(111)$ model, with the reactants sequence $CO \rightarrow O_2 \rightarrow CO$, beginning with removing O atoms from the top layer of the Pt_6O_9 cluster. The shown energy corresponds to the energy change with respect to the previous step in the reaction coordinate; the values displayed in green are the activation energies.

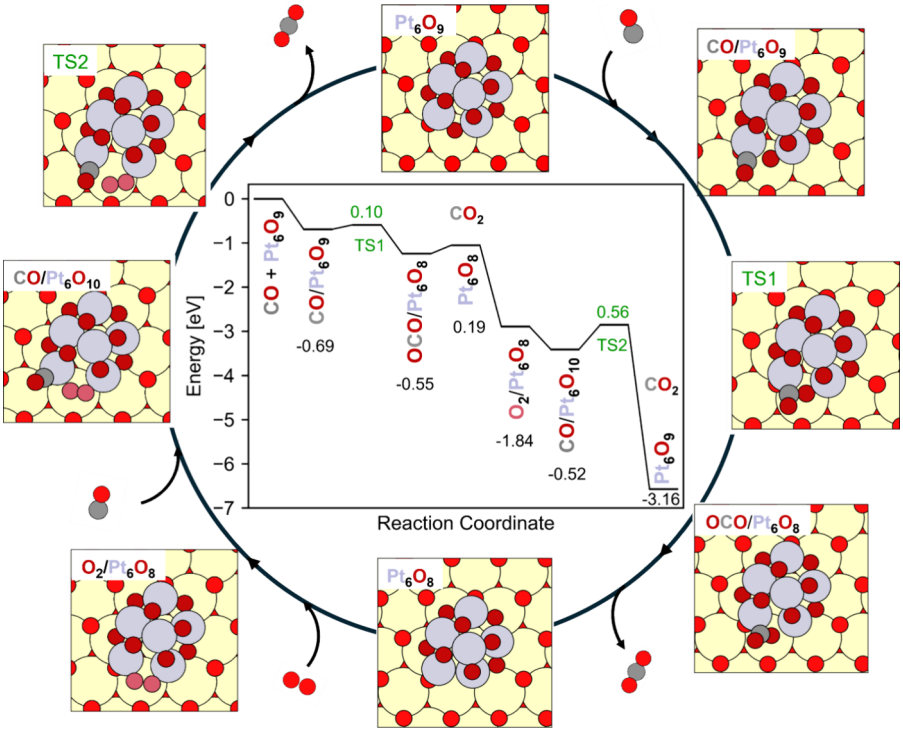

Figure 4. Calculated energies and structures of path #3 for CO oxidation on the $Pt_6O_9/CeO_2(111)$ model, with the reactants sequence $CO \rightarrow O_2 \rightarrow CO$ and which begins removing an O atom from the bottom (interface) layer of the Pt_6O_9 cluster. The energy values correspond to the energy change with respect to the previous step in the reaction coordinate; the values displayed in green are the activation energies.

https://doi.org/10.1021/acscatal.6c01003
ACS Catal. 2026, 16, 12009−12020

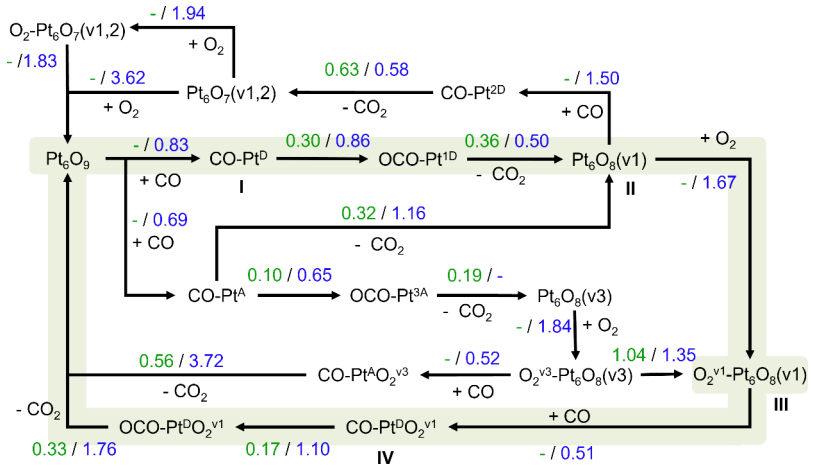

Figure 5. Calculated activation barriers (in eV) of the reaction network studied for the low-temperature CO oxidation catalyzed by Pt_6O_9/CeO_2. Forward barriers are in green while backward barriers are in blue. The catalytic cycle with the lowest barriers along the reaction path is highlighted.

in magnitude to –0.21 eV, which justifies neglecting the high-coverage situation in the kMC simulations.

The considered reactions for the kMC simulations are:

$$Pt_6O_9 + CO \leftrightarrow CO(D)\text{–}Pt_6O_9 \qquad (R1 - TL)$$

$$Pt_6O_9 + CO \leftrightarrow CO(A)\text{–}Pt_6O_9 \qquad (R1 - BL)$$

$$CO(D) - Pt_6O_9 \leftrightarrow O(1) - CO(D) - Pt_6O_9 \qquad (R2 - TL)$$

$$CO(A) - Pt_6O_9 \leftrightarrow O(3) - CO(A) - Pt_6O_9 \qquad (R2 - BL)$$

$$O(1) - CO(D) - Pt_6O_8 \rightarrow Pt_6O_8(v1) + CO_2 \qquad (R3 - TL)$$

$$O(3) - CO(A) - Pt_6O_8 \rightarrow Pt_6O_8(v3) + CO_2 \qquad (R3 - BL)$$

$$Pt_6O_8(v1) + O_2 \leftrightarrow Pt_6O_{10}(v1) \qquad (R4 - TL)$$

$$Pt_6O_8(v3) + O_2 \leftrightarrow Pt_6O_{10}(v3) \qquad (R4 - BL)$$

$$Pt_6O_{10}(v1) + CO \leftrightarrow CO(D) - Pt_6O_{10}(v1) \qquad (R5 - TL)$$

$$Pt_6O_{10}(v3) + CO \leftrightarrow CO(A) - Pt_6O_{10}(v3) \qquad (R5 - BL)$$

$$CO(D) - Pt_6O_{10}(v1) \leftrightarrow O - CO(D) - Pt_6O_9(v1) \qquad (R5.5 - TL)$$

$$O - CO(D) - Pt_6O_9(v1) \rightarrow CO_2 + Pt_6O_9 \qquad (R6 - TL)$$

$$O - CO(A) - Pt_6O_9(v3) \rightarrow CO_2 + Pt_6O_9 \qquad (R6 - BL)$$

R1–R6 are steps of the catalytic cycles with the $CO \rightarrow O_2 \rightarrow CO$ reactant sequence. TL and BL labels indicate catalytic cycles involving the top layer (distant from the support) and bottom layer (nearest to the support or *interface*) O atoms of the Pt_6O_9 cluster, respectively. R1 and R5 are CO adsorption steps, R2 and R5.5 (for the top layer cycle) are CO activation steps forming O–CO complexes. R3 and R6 are CO_2 desorption steps. R4 is O_2 adsorption on the vacancy site created by the CO_2 desorption R3.

From the kMC simulations as a function of temperature (using zero-point energy corrected DFT data shown in Table S3 obtained from vibrational frequency contributions), we obtain the turnover frequency (TOF) per Pt site from –70 to 80 °C as shown in Figure 6. These simulations reveal that CO oxidation becomes active for the top layer cycle at –70 °C. Notably, for this reaction pathway, the TOF of ca. 10^4 s^{-1} at –40 °C is close to that calculated at ca. 200 °C for CO oxidation on the catalytically active small metallic Pt particles supported on $CeO_2(111)$.[52] The TOF values of the bottom layer cycle are consistently smaller by 2–3 orders of magnitude than the values of the top layer cycle in the studied temperature range.

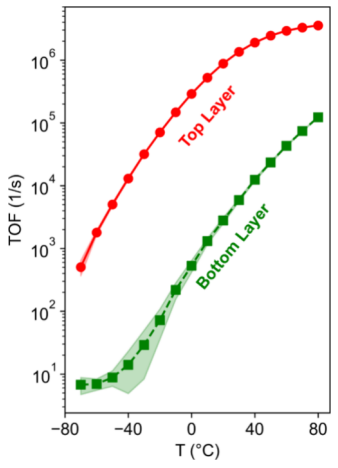

Figure 6. Calculated turnover frequencies (TOF) derived from kMC simulations at –70 to 80 °C for CO oxidation over the $Pt_6O_9/CeO_2(111)$ model in the top-layer and bottom-layer catalytic cycles described in Figures 3 and 4, respectively. The shaded area in each curve corresponds to the standard deviation calculated from data shown in Table S5 (Top Layer mechanism) and Table S6 (Bottom Layer mechanism). The partial pressures of CO and O_2 are 6×10^{-3} and 1×10^{-2} atm, respectively, to mimic the experimental conditions.[43]

https://doi.org/10.1021/acscatal.6c01003
ACS Catal. 2026, 16, 12009–12020

To further relate the kMC simulations results to the experimental data, apparent activation energies are calculated for each mechanism in the temperature range from −40 to 40 °C, where the Arrhenius plots for both mechanisms exhibit a linear correlation between ln(k) and 1/T (Figure S3). The calculated apparent activation energy is 0.40 eV for the more efficient top layer and 0.54 eV for the bottom layer. Apparent activation energies at this temperature range follow well, as expected, the highest barriers of the two mechanisms (0.41 and 0.56 eV for the top -layer and bottom- layer cycles respectively, as corrected with the ZPE values shown in Table S3).

4. CONCLUSIONS

The CO oxidation activity of ceria-supported PtO_x particles below room temperature has been studied using DFT calculations and kinetic Monte Carlo simulations of a Pt_6O_9/CeO_2(111) model system. The Pt_6O_9 cluster contains reactive oxygen atoms with smaller O vacancy formation energies than those of the CeO_2(111) support at the interface with the cluster. The high CO oxidation activity at remarkably low temperatures results from interactions of such mobile O atoms of the Pt_6O_9 cluster with CO molecules adsorbed on it, forming, with low reaction barriers of ≥0.10 eV, weakly bound CO_2 species that thereafter easily desorb. The activation of O_2 molecules, which is often reported as the rate-determining step in catalysts based on oxidized Pt catalysts on ceria,[38] also proceeds through low barriers by healing the created O vacancies in the cluster and providing an extra O atom for the oxidation of an additional CO molecule with activation energies starting from 0.17 eV.

The mechanism involving O atoms from the top layer of the Pt_6O_9 cluster exhibits lower barriers than the mechanism involving O atoms of the Pt_6O_9 cluster located at the PtO_x/ceria interface in direct contact with the support. This is in contrast to the often-assumed higher reactivity of interface sites in ceria-supported metal catalysts.

Our kinetic Monte Carlo simulations demonstrate that the discovered paths are consistent with high TOF at temperatures as low as −40 °C. The obtained TOF values are close to those obtained at ca. 200 °C higher temperatures in kMC simulations of CO oxidation on metallic (not oxidized) Pt particles supported on CeO_2(111).[52] Therefore, the remarkable CO oxidation activity measured for some Pt/CeO_2 catalysts below room temperature is attributed to the presence of PtO_x particles, whose O atoms can efficiently be consumed to produce CO_2 with the subsequent healing of the oxygen vacancies by molecular O_2. Unlike conventional MvK mechanisms, in which the oxide support CeO_2 provides reactive oxygen, in the present very-low temperature mechanism (also of a MvK kind, but with reactive O from PtO_x), the CeO_2 support appears to be merely a spectator.

The key prerequisite for high activity of the studied here Pt/CeO_2 catalysts in CO oxidation at very low temperature is the PtO_x species moderately weakly adsorbing CO molecules without poisoning of active sites while offering reactive oxygen near adsorbed CO. The main findings of this study are generalizable to conventional Pt/CeO_2 catalysts, which can potentially exhibit PtO_x clusters and the resulting low-temperature CO oxidation activity when subjected to well-designed preparation and redox pretreatment strategies.[43,45] If PtO_x particles exhibiting [PtO_4] motifs can be anchored to other less reactive supports, they are expected to also mediate the low-temperature CO oxidation. Other transition metals, which are less electronegative than noble metal Pt, easily form metal-oxide MO_x species containing reactive oxygen required for the low-temperature CO oxidation. For instance, noble metal-free catalysts based on cobalt-oxide Co_3O_4 are active in CO oxidation at the extraordinarily low temperature below −70 °C.[70,71] These similarities in the low-temperature oxidation activity mediated by noble and not noble metal-oxide species imply a general character of the insights provided in this study about the underlying catalytic mechanisms. Thus, the present study can open new ways for designing efficient catalysts for oxidation reactions occurring at very low temperatures, which are not necessarily based on scarce precious noble metals.

■ ASSOCIATED CONTENT

Data Availability Statement

Output files of the calculations performed in this study are openly available in the ioChem-BD repository[72] at 10.19061/iochem-bd-6-655.

Supporting Information

The Supporting Information is available free of charge at https://pubs.acs.org/doi/10.1021/acscatal.6c01003.

CO oxidation catalytic cycle following the reactants sequence CO/CO/O_2; structural parameters and vibrational frequencies of CO adsorption complexes; formation energies of the second O vacancy; reactive events considered in kinetic Monte Carlo simulations and the corresponding activation energies used; dependence of the TOF on the simulation time; statistics data of the TOF calculations; details of the apparent activation energy calculations (PDF)

■ AUTHOR INFORMATION

Corresponding Authors

Albert Bruix – *Departament de Ciència de Materials i Química Física & Institut de Quimica Teòrica i Computacional (IQTCUB), Universitat de Barcelona, Barcelona 08028, Spain*; orcid.org/0000-0003-2585-5542; Email: abruix@ub.edu

Konstantin M. Neyman – *Departament de Ciència de Materials i Química Física & Institut de Quimica Teòrica i Computacional (IQTCUB), Universitat de Barcelona, Barcelona 08028, Spain; ICREA (Institució Catalana de Recerca i Estudis Avançats), Barcelona 08010, Spain*; orcid.org/0000-0002-5242-5567; Email: konstantin.neyman@icrea.cat

Authors

Pablo Castro-Latorre – *Departament de Ciència de Materials i Química Física & Institut de Quimica Teòrica i Computacional (IQTCUB), Universitat de Barcelona, Barcelona 08028, Spain*; orcid.org/0000-0003-3763-5766

Henrik Grönbeck – *Competence Centre for Catalysis, Chalmers University of Technology, Göteborg 41296, Sweden*

Complete contact information is available at: https://pubs.acs.org/doi/10.1021/acscatal.6c01003

Notes

The authors declare no conflict of interest.

https://doi.org/10.1021/acscatal.6c01003
ACS Catal. 2026, 16, 12009−12020

■ ACKNOWLEDGMENTS

Authors acknowledge financial support from Spanish/FEDER *Ministerio de Ciencia, Innovación y Universidades* (grants PRE2019-088979 (for P.C.L.), PID2021-128217NB-I00, PID2022-140120OA-I00, PID2024-157317NB-I00 and CEX 2021-001202-M and RYC2021-032281-I (for A.B.)); *Generalitat de Catalunya* (grant 2021SGR00286); Swedish Research Council (2024-05250). This study was supported the by the COST Actions CA18234 and CA21101 and by the International Research Network IRN Nanoalloys (CNRS). Computational time was provided by the *Red Española de Supercomputación* and the National Academic Infrastructure for Super-computing in Sweden (2025/3-36). P.C.L acknowledge Rasmus Svensson for his helpful insights on the MonteCoffee code.

■ REFERENCES

(1) Gandhi, H. S.; Graham, G. W.; McCabe, R. W. Automotive Exhaust Catalysis. *J. Catal.* **2003**, *216*, 433–442.
(2) Kašpar, J.; Fornasiero, P.; Hickey, N. Automotive catalytic converters: current status and some perspectives. *Catal. Today* **2003**, *77*, 419.
(3) Freund, H. J.; Meijer, G.; Scheffler, M.; Schlögl, R.; Wolf, M. CO Oxidation as a Prototypical Reaction for Heterogeneous Processes. *Angew. Chem. Int. Ed.* **2011**, *50* (43), 10064–10094.
(4) Liebertseder, M.; Maliakkal, C. B.; Crone, M.; Nails, G.; Casapu, M.; Grunwaldt, J. D.; Türk, M.; Kübel, C.; Feldmann, C. TiO_2−CeO_x−Pt Hollow Nanosphere Catalyst for Low-Temperature CO Oxidation. *ChemCatChem* **2024**, *16* (2), No. e202301358.
(5) Dononelli, W.; Moskaleva, L. V.; Klüner, T. CO Oxidation over Unsupported Group 11 Metal Catalysts: New Mechanistic Insight from First-Principles. *J. Phys. Chem. C* **2019**, *123* (13), 7818–7830.
(6) Zhang, J.; Shu, M.; Niu, Y.; Yi, L.; Yi, H.; Zhou, Y.; Zhao, S.; Tang, X.; Gao, F. Advances in CO Catalytic Oxidation on Typical Noble Metal Catalysts: Mechanism, Performance and Optimization. *Chem. Eng. J.* **2024**, *495*, No. 153523.
(7) Royer, S.; Duprez, D. Catalytic Oxidation of Carbon Monoxide over Transition Metal Oxides. *ChemCatChem* **2011**, *3* (1), 24–65.
(8) Tang, X.; Tariq, N. H.; Wang, J.; Cheng, Y.; Wang, Y.; Yuan, Z.; Liu, B. CuO/TiO_2/Ti Monolithic Catalysts for Low-Temperature CO Oxidation. *ACS Appl. Nano Mater.* **2024**, *7* (1), 809–817.
(9) Liu, S.; Xue, Y.; Jia, Y.; Wang, H.; Nie, Q.; Fan, J. Catalytic CO Oxidation on CeO_2-Based Materials: Modification Strategies, Structure-Performance Relationships, Challenges and Prospects. *Sep. Purif. Technol.* **2025**, *359*, No. 130556.
(10) Rodriguez, J. A.; Grinter, D. C.; Liu, Z.; Palomino, R. M.; Senanayake, S. D. Ceria-Based Model Catalysts: Fundamental Studies on the Importance of the Metal-Ceria Interface in CO Oxidation, the Water-Gas Shift, CO_2 Hydrogenation, and Methane and Alcohol Reforming. *Chem. Soc. Rev.* **2017**, *46* (7), 1824–1841.
(11) Pauletti, C. F.; Farnesi Camellone, M.; Piccinin, S. Influence of Local Chemical Environment on the Catalytic Properties of Ir_1/CeO_2 Single-Atom Catalysts in CO Oxidation. *ACS Catal.* **2025**, *15* (7), 5806–5824.
(12) Li, Z.; Haynes, B. S.; Montoya, A. Carbon Monoxide Oxidation on Ceria-Supported Nanoclusters. *ACS Appl. Mater. Interfaces* **2023**, *15* (44), 51885–51893.
(13) Yuan, K.; Guo, Y.; Huang, L.; Zhou, L.; Yin, H. J.; Liu, H.; Yan, C. H.; Zhang, Y. W. Tunable Electronic Metal-Support Interactions on Ceria-Supported Noble-Metal Nanocatalysts in Controlling the Low-Temperature CO Oxidation Activity. *Inorg. Chem.* **2021**, *60* (7), 4207–4217.
(14) Lustemberg, P. G.; Yang, C.; Wang, Y.; Ganduglia-Pirovano, M. V.; Wöll, C. Synergistic Effects in Low-Temperature CO Oxidation on Cerium Oxide Surfaces. *J. Am. Chem. Soc.* **2025**, *147* (8), 6958–6965.
(15) Neyman, K. M.; Kozlov, S. M. Quantifying Interactions on Interfaces between Metal Particles and Oxide Supports in Catalytic Nanomaterials. *NPG Asia Mater.* **2022**, *14* (1), No. 59.
(16) Stadnichenko, A. I.; Slavinskaya, E. M.; Stonkus, O. A.; Boronin, A. I. Low-Temperature CO Oxidation by the Pt/CeO_2 Based Catalysts. *ChemCatChem* **2024**, *16* (15), No. e202301727.
(17) Li, Z.; Liu, Z.; Gao, G.; Zhao, W.; Jiang, Y.; Tang, X.; Dai, S.; Qu, Z.; Yan, N.; Ma, L. Enhanced Catalytic Oxidation Reactivity over Atomically Dispersed Pt/CeO_2 Catalysts by CO Activation. *Environ. Sci. Technol.* **2024**, *58* (27), 12201–12211.
(18) Kauppinen, M. M.; Daelman, N.; López, N.; Honkala, K. The Role of Polaronic States in the Enhancement of CO Oxidation by Single-Atom Pt/CeO_2. *J. Catal.* **2023**, *423*, 26–33.
(19) Li, B.; Li, J.; Ding, S.; Su, Y. Theoretical Study on Pt_1/CeO_2 Single Atom Catalysts for CO Oxidation. *ChemCatChem* **2025**, *17* (4), No. e202401494.
(20) Zhang, Z.; Tian, J.; Lu, Y.; Yang, S.; Jiang, D.; Huang, W.; Li, Y.; Hong, J.; Hoffman, A. S.; Bare, S R; Engelhard, M. H.; Datye, A. K.; Wang, Y. Memory-Dictated Dynamics of Single-Atom Pt on CeO_2 for CO Oxidation. *Nat. Commun.* **2023**, *14* (1), No. 2664.
(21) Xiao, Y.; Li, H.; Xie, K. Activating Lattice Oxygen at the Twisted Surface in a Mesoporous CeO_2 Single Crystal for Efficient and Durable Catalytic CO Oxidation. *Angew. Chem. Int. Ed.* **2021**, *60* (10), 5240–5244.
(22) Koleva, I. Z.; Aleksandrov, H. A.; Vayssilov, G. N. Comparison of the Reactivity of Platinum Cations and Clusters Supported on Ceria or Alumina in Carbon Monoxide Oxidation. *ACS Catal.* **2023**, *13* (8), 5358–5374.
(23) Kunz, S.; Schweinberger, F. F.; Habibpour, V.; Röttgen, M.; Harding, C.; Arenz, M.; Heiz, U. Temperature Dependent CO Oxidation Mechanisms on Size-Selected Clusters. *J. Phys. Chem. C* **2010**, *114* (3), 1651–1654.
(24) Meher, S. K.; Cargnello, M.; Troiani, H.; Montini, T.; Rao, G. R.; Fornasiero, P. Alcohol Induced Ultra-Fine Dispersion of Pt on Tuned Morphologies of CeO_2 for CO Oxidation. *Appl. Catal. B, Environ.* **2013**, *130*−*131*, 121–131.
(25) Maurer, F.; Beck, A.; Jelic, J.; Wang, W.; Mangold, S.; Stehle, M.; Wang, D.; Dolcet, P.; Gänzler, A. M.; Kübel, C.; Studt, F.; Casapu, M.; Grunwaldt, J. D. Surface Noble Metal Concentration on Ceria as a Key Descriptor for Efficient Catalytic CO Oxidation. *ACS Catal.* **2022**, *12* (4), 2473–2486.
(26) Chen, C.; Chen, J. L.; Feng, L.; Hu, J.; Chai, X.; Liu, J. X.; Li, W. X. Reactant-Induced Dynamic Stabilization of Highly Dispersed Pt Catalysts on Ceria Dictating the Reactivity of CO Oxidation. *ACS Catal.* **2024**, *14* (5), 3504–3513.
(27) Ferré, G.; Aouine, M.; Bosselet, F.; Burel, L.; Cadete Santos Aires, F. J.; Geantet, C.; Ntais, S.; Maurer, F.; Casapu, M.; Grunwaldt, J. D.; Epicier, T.; Loridant, S.; Vernoux, P. Exploiting the Dynamic Properties of Pt on Ceria for Low-Temperature CO Oxidation. *Catal. Sci. Technol.* **2020**, *10* (12), 3904–3917.
(28) Meunier, F. C.; Cardenas, L.; Kaper, H.; Šmíd, B.; Vorokhta, M.; Grosjean, R.; Aubert, D.; Dembélé, K.; Lunkenbein, T. Synergy between Metallic and Oxidized Pt Sites Unravelled during Room Temperature CO Oxidation on Pt/Ceria. *Angew. Chem. Int. Ed.* **2021**, *60* (7), 3799–3805.
(29) Simanenko, A.; Kastenmeier, M.; Piliai, L.; Kosto, Y.; Skála, T.; Tsud, N.; Mehl, S.; Vorokhta, M.; Matolínová, I.; Lykhach, Y.; Libuda, J. Probing the Redox Capacity of Pt-CeO2 Model Catalyst for Low-Temperature CO Oxidation. *J. Mater. Chem. A* **2023**, *11* (31), 16659–16670.
(30) Yang, Y.; Yi, X.; Deng, L.; Zhao, Z.; Liu, Z.; Li, M.; Dou, B.; Bin, F. Promoting Oxidation of High Concentration CO via Strong Metal Support Interaction in Unreduced Pt-Based Catalysts. *J. Environ. Chem. Eng.* **2025**, *13* (3), No. 116472.
(31) Borges, L. R.; da Silva, A. G. M.; Braga, A. H.; Rossi, L. M.; Suller Garcia, M. A.; Vidinha, P. Towards the Effect of $Pt^0/Pt^{\delta+}$ and Ce^{3+} Species at the Surface of CeO_2 Crystals: Understanding the Nature of the Interactions under CO Oxidation Conditions. *ChemCatChem* **2021**, *13* (5), 1340–1354.

https://doi.org/10.1021/acscatal.6c01003
ACS Catal. 2026, 16, 12009−12020

(32) Lv, Y.; Li, A.; Ye, J.; Wang, H.; Hu, P.; Wang, K. W.; Guo, Y.; Tang, X.; Dai, S. Exploring the Facet-Dependent Structural Evolution of Pt/CeO_2 Catalysts Induced by Typical Pretreatments for CO Oxidation. *ACS Appl. Mater. Interfaces* **2024**, *16* (33), 43556–43564.
(33) Liotta, L. F.; Longo, A.; Pantaleo, G.; Di Carlo, G.; Martorana, A.; Cimino, S.; Russo, G.; Deganello, G. Alumina Supported Pt(1%)/$Ce_{0.6}Zr_{0.4}O_2$ Monolith: Remarkable Stabilization of Ceria-Zirconia Solution towards $CeAlO_3$ Formation Operated by Pt under Redox Conditions. *Appl. Catal. B, Environ.* **2009**, *90* (3−4), 470–477.
(34) Song, S.; Wu, Y.; Ge, S.; Wang, L.; Wang, Y.; Guo, Y.; Zhan, W.; Guo, Y. A Facile Way to Improve Pt Atom Efficiency for CO Oxidation at Low Temperature: Modification by Transition Metal Oxides. *ACS Catal.* **2019**, *9* (7), 6177–6187.
(35) Imanaka, N.; Masui, T.; Imadzu, H.; Yasuda, K. Carbon Monoxide Oxidation at Room Temperature on Pt/CeO_2-ZrO_2-Bi_2O_3 Catalysts. *Chem. Commun.* **2011**, *47* (39), 11032–11034.
(36) Beg, M. B.; Ali, L.; Shittu, T.; Khaleel, A.; Vermeire, F. H.; Altarawneh, M. Non-Noble Catalysts Formulations Using CuO-CeO_2/Nb_2O_5 for Low-Temperature Catalytic Oxidation of Carbon Monoxide. *J. Environ. Chem. Eng.* **2024**, *12* (4), No. 113177.
(37) Quinlivan Domínguez, J. E.; Neyman, K. M.; Bruix, A. Stability of Oxidized States of Freestanding and Ceria-Supported PtO_x particles. *J. Chem. Phys.* **2022**, *157* (9), No. 094709.
(38) Wang, H.; Liu, J. X.; Allard, L. F.; Lee, S.; Liu, J.; Li, H.; Wang, J.; Wang, J.; Oh, S. H.; Li, W.; Flytzani-Stephanopoulos, M.; Shen, M.; Goldsmith, B. R.; Yang, M. Surpassing the Single-Atom Catalytic Activity Limit through Paired Pt-O–Pt Ensemble Built from Isolated Pt_1 Atoms. *Nat. Commun.* **2019**, *10* (1), No. 3808.
(39) Zhou, H.; Su, N. Q. From Single Atoms to Clusters: Unraveling the Structural Evolution of Pt/CeO_2 for Enhanced CO Oxidation. *J. Phys. Chem. Lett.* **2025**, *16* (11), 2845–2855.
(40) Ke, J.; Zhu, W.; Jiang, Y.; Si, R.; Wang, Y. J.; Li, S. C.; Jin, C.; Liu, H.; Song, W. G.; Yan, C. H.; Zhang, Y. W. Strong Local Coordination Structure Effects on Subnanometer PtO_x Clusters over CeO_2 Nanowires Probed by Low-Temperature CO Oxidation. *ACS Catal.* **2015**, *5* (9), 5164–5173.
(41) Dong, J.; Zhang, Y.; Li, D.; Adogwa, A.; Huang, S.; Yang, M.; Yang, J.; Jin, Q. Reaction-Driven Evolutions of Pt States over Pt-CeO_2 Catalysts during CO Oxidation. *Appl. Catal. B Environ.* **2023**, *330*, No. 122662.
(42) Yohannes, A. G.; Fink, K.; Kondov, I. Pt Nanoparticles under Oxidizing Conditions - Implications of Particle Size, Adsorption Sites and Oxygen Coverage on Stability. *Nanoscale Adv.* **2022**, *4*, 4554–4569.
(43) Slavinskaya, E. M.; Stadnichenko, A. I.; Quinlivan Domínguez, J. E.; Stonkus, O. A.; Vorokhta, M.; Šmíd, B.; Castro-Latorre, P.; Bruix, A.; Neyman, K. M.; Boronin, A. I. States of Pt/CeO_2 Catalysts for CO Oxidation below Room Temperature. *J. Catal.* **2023**, *421*, 285–299.
(44) Yan, J.; Dai, Q.; Wang, H.; Wang, Z.; Yu, J.; Dai, S.; Monai, M.; Weckhuysen, B. M.; Zhan, W. Enhanced CO Oxidation on PtO_x Raft Species Synthesized via Citric Acid-Assisted Electrostatic Adsorption. *Angew. Chem. Int. Ed.* **2025**, *65* (2), No. e20136.
(45) Boronin, A. I.; Slavinskaya, E. M.; Figueroba, A.; Stadnichenko, A. I.; Kardash, T. Y.; Stonkus, O. A.; Fedorova, E. A.; Muravev, V. V.; Svetlichnyi, V. A.; Bruix, A.; Neyman, K. M. CO Oxidation Activity of Pt/CeO_2 Catalysts below 0 °C: Platinum Loading Effects. *Appl. Catal. B Environ.* **2021**, *286*, No. 119931.
(46) Wang, Y.; Pei, C.; Zhao, Z.-J.; Gong, J. Kinetically Rate-Determining Step Modulation by Metal—Support Interactions for CO Oxidation on Pt/CeO_2. *Sci. China Chem.* **2022**, *65* (10), 2038–2044.
(47) Lu, Y.; Thompson, C.; Kunwar, D.; Datye, A. K.; Karim, A. M. Origin of the High CO Oxidation Activity on CeO_2 Supported Pt Nanoparticles: Weaker Binding of CO or Facile Oxygen Transfer from the Support?. *ChemCatChem* **2020**, *12* (6), 1726–1733.
(48) Liu, X.; Jia, S.; Yang, M.; Tang, Y.; Wen, Y.; Chu, S.; Wang, J.; Shan, B.; Chen, R. Activation of Subnanometric Pt on Cu-Modified CeO_2 via Redox-Coupled Atomic Layer Deposition for CO Oxidation. *Nat. Commun.* **2020**, *11* (1), No. 4240.
(49) Cargnello, M.; Doan-Nguyen, V. V. T.; Gordon, T. R.; Diaz, R. E.; Stach, E. A.; Gorte, R. J.; Fornasiero, P.; Murray, C. B. Control of Metal Nanocrystal Size Reveals Metal-Support Interface Role for Ceria Catalysts. *Science* **2013**, *341* (6147), 771–773.
(50) An, K.; Alayoglu, S.; Musselwhite, N.; Plamthottam, S.; Melaet, G.; Lindeman, A. E.; Somorjai, G. A. Enhanced CO Oxidation Rates at the Interface of Mesoporous Oxides and Pt Nanoparticles. *J. Am. Chem. Soc.* **2013**, *135* (44), 16689–16696.
(51) Wang, Y.; Ma, J.; Wang, X.; Zhang, Z.; Zhao, J.; Yan, J.; Du, Y.; Zhang, H.; Ma, D. Complete CO Oxidation by O_2 and H_2O over Pt-$CeO_{2-\delta}$/MgO Following Langmuir-Hinshelwood and Mars-van Krevelen Mechanisms, Respectively. *ACS Catal.* **2021**, *11* (19), 11820–11830.
(52) Bosio, N.; Di, M.; Skoglundh, M.; Carlsson, P. A.; Grönbeck, H. Interface Reactions Dominate Low-Temperature CO Oxidation Activity over Pt/CeO_2. *J. Phys. Chem. C* **2022**, *126* (38), 16164–16171.
(53) Resasco, J.; DeRita, L.; Dai, S.; Chada, J. P.; Xu, M.; Yan, X.; Finzel, J.; Hanukovich, S.; Hoffman, A. S.; Graham, G. W.; Bare, S. R.; Pan, X.; Christopher, P. Uniformity Is Key in Defining Structure−Function Relationships for Atomically Dispersed Metal Catalysts: The Case of Pt/CeO_2. *J. Am. Chem. Soc.* **2020**, *142* (1), 169–184.
(54) Kopelent, R.; van Bokhoven, J. A.; Szlachetko, J.; Edebeli, J.; Paun, C.; Nachtegaal, M.; Safonova, O. V. Catalytically Active and Spectator Ce^{3+} in Ceria-Supported Metal Catalysts. *Angew. Chem. Int. Ed.* **2015**, *54* (30), 8728–8731.
(55) Kardash, T. Y.; Derevyannikova, E. A.; Slavinskaya, E. M.; Stadnichenko, A. I.; Maltsev, V. A.; Zaikovskii, A. V.; Novopashin, S. A.; Boronin, A. I.; Neyman, K. M. Pt/CeO_2 and Pt/$CeSnO_x$ Catalysts for Low-Temperature CO Oxidation Prepared by Plasma-Arc Technique. *Front. Chem.* **2019**, *7*, 114.
(56) Wang, C.; Gu, X.-K.; Yan, H.; Lin, Y.; Li, J.; Liu, D.; Li, W.-X.; Lu, J. Water-Mediated Mars−Van Krevelen Mechanism for CO Oxidation on Ceria-Supported Single-Atom Pt_1 Catalyst. *ACS Catal.* **2017**, *7* (1), 887–891.
(57) Pereira-Hernández, X. I.; DeLaRiva, A.; Muravev, V.; Kunwar, D.; Xiong, H.; Sudduth, B.; Engelhard, M.; Kovarik, L.; Hensen, E. J. M.; Wang, Y.; Datye, A. K. Tuning Pt-CeO_2 Interactions by High-Temperature Vapor-Phase Synthesis for Improved Reducibility of Lattice Oxygen. *Nat. Commun.* **2019**, *10* (1), No. 1358.
(58) Nie, L.; Mei, D.; Xiong, H.; Peng, B.; Ren, Z.; Hernandez, X. I. P.; DeLaRiva, A.; Wang, M.; Engelhard, M. H.; Kovarik, L.; Datye, A. K.; Wang, Y. Activation of Surface Lattice Oxygen in Single-Atom Pt/CeO_2 for Low-Temperature CO Oxidation. *Science* **2017**, *358* (6369), 1419–1423.
(59) Kresse, G.; Furthmüller, J. Efficiency of Ab-Initio Total Energy Calculations for Metals and Semiconductors Using a Plane-Wave Basis Set. *Comput. Mater. Sci.* **1996**, *6* (1), 15–50.
(60) Kresse, G.; Furthmüller, J. Efficient Iterative Schemes for Ab Initio Total-Energy Calculations Using a Plane-Wave Basis Set. *Phys. Rev. B Condens. Matter Mater. Phys.* **1996**, *54* (16), 11169–11186.
(61) Kresse, G.; Hafner, J. Ab Initio Molecular Dynamics for Liquid Metals. *Phys. Rev. B* **1993**, *47* (1), 558–561.
(62) Blöchl, P. E. Projector Augmented-Wave Method. *Phys. Rev. B* **1994**, *50* (24), 17953–17979.
(63) Perdew, J. P.; Wang, Y. Accurate and Simple Analytic Representation of the Electron-Gas Correlation Energy. *Phys. Rev. B* **1992**, *45* (23), 13244–13249.
(64) Anisimov, V. I.; Aryasetiawan, F.; Lichtenstein, A. I. First-Principles Calculations of the Electronic Structure and Spectra of Strongly Correlated Systems: The LDA + U Method. *J. Phys. Condens. Matter* **1997**, *9* (4), 767–808.
(65) Loschen, C.; Carrasco, J.; Neyman, K. M.; Illas, F. First-Principles LDA+U and GGA+U Study of Cerium Oxides: Dependence on the Effective U Parameter. *Phys. Rev. B* **2007**, *75* (3), No. 035115.
(66) Henkelman, G.; Uberuaga, B. P.; Jónsson, H. Climbing Image Nudged Elastic Band Method for Finding Saddle Points and Minimum Energy Paths. *J. Chem. Phys.* **2000**, *113* (22), 9901–9904.

https://doi.org/10.1021/acscatal.6c01003
ACS Catal. 2026, 16, 12009−12020

(67) Jansen, A. P. J. *An Introduction to Kinetic Monte Carlo Simulations of Surface Reactions*; Lecture Notes in Physics; Springer Berlin Heidelberg: Berlin, Heidelberg, **2012**; *Vol 856.*
(68) Jørgensen, M.; Grönbeck, H. MonteCoffee: A Programmable Kinetic Monte Carlo Framework. *J. Chem. Phys.* **2018**, *149* (11), No. 114101.
(69) Bruix, A.; Migani, A.; Vayssilov, G. N.; Neyman, K. M.; Libuda, J.; Illas, F. Effects of Deposited Pt Particles on the Reducibility of CeO_2(111). *Phys. Chem. Chem. Phys.* **2011**, *13* (23), No. 11384.
(70) Xie, X.; Li, Y.; Liu, Z.-Q.; Haruta, M.; Shen, W. Low-Temperature Oxidation of CO Catalysed by Co_3O_4 Nanorods. *Nature* **2009**, *458* (7239), 746–749.
(71) Jia, C.-J.; Schwickardi, M.; Weidenthaler, C.; Schmidt, W.; Korhonen, S.; Weckhuysen, B. M.; Schüth, F. Co_3O_4–SiO_2 Nanocomposite: A Very Active Catalyst for CO Oxidation with Unusual Catalytic Behavior. *J. Am. Chem. Soc.* **2011**, *133* (29), 11279–11288.
(72) Álvarez-Moreno, M.; de Graaf, C.; López, N.; Maseras, F.; Poblet, J. M.; Bo, C. Managing the Computational Chemistry Big Data Problem: The IoChem-BD Platform. *J. Chem. Inf. Model.* **2015**, *55* (1), 95–103.

https://doi.org/10.1021/acscatal.6c01003
ACS Catal. 2026, 16, 12009–12020